



Lawrence Berkeley Laboratory

UNIVERSITY OF CALIFORNIA

EARTH SCIENCES DIVISION

To be presented at the Society of Petroleum Engineers California
Regional Meeting, Bakersfield, CA, April 5-7, 1989,
and to be published in the Proceedings

A Laboratory Investigation of Foam Flow in Sandstone at Elevated Pressure

P. Persoff, C.J. Radke, K. Pruess, S.M. Benson,
and P.A. Witherspoon

January 1989



1 LOAN COPY 1
1 Circulates 1
1 for 4 weeks 1

Bldg. 50 Library. 2

LBL-26639

DISCLAIMER

This document was prepared as an account of work sponsored by the United States Government. While this document is believed to contain correct information, neither the United States Government nor any agency thereof, nor the Regents of the University of California, nor any of their employees, makes any warranty, express or implied, or assumes any legal responsibility for the accuracy, completeness, or usefulness of any information, apparatus, product, or process disclosed, or represents that its use would not infringe privately owned rights. Reference herein to any specific commercial product, process, or service by its trade name, trademark, manufacturer, or otherwise, does not necessarily constitute or imply its endorsement, recommendation, or favoring by the United States Government or any agency thereof, or the Regents of the University of California. The views and opinions of authors expressed herein do not necessarily state or reflect those of the United States Government or any agency thereof or the Regents of the University of California.

**A Laboratory Investigation of Foam Flow
in Sandstone at Elevated Pressure**

P. Persoff,^{} C. J. Radke,^{*,†} K. Pruess,^{*} S. M. Benson,^{*} and P. A. Witherspoon^{*,‡}*

^{*}Earth Sciences Division
Lawrence Berkeley Laboratory
University of California
Berkeley, California 94720

[†]Chemical Engineering Department
University of California

[‡]Materials Science and Mineral Engineering Department
University of California

January 1989

ABSTRACT

Use of foam as a mobility-control fluid in underground applications such as enhanced oil recovery and natural gas or air storage in aquifers requires quantitative information on its flow behavior in porous media at relevant conditions. Little information is currently available in consolidated sands and at pressures characteristic of reservoir depths. We study the flow of foam through a $1.3 \mu\text{m}^2$ Boise sandstone core at ambient temperature and at back pressures up to 5.2 MPa (750 psia). Total superficial velocities range from 1 to 45 m/day, and inlet foam qualities range from 0.70 to 0.996. Sequential pressure taps and gamma-ray attenuation are used to measure local flow resistances and liquid saturations during transient displacement and in the steady state.

We find that foam in the unsteady state is rheopectic; in the steady state it is shear thinning with respect to increasing gas flow but Newtonian with respect to increasing liquid flow. That is, steady pressure gradients for foam are sensibly independent of gas velocity but increase nearly linearly with increasing liquid velocity. No hysteresis in foam flow resistance is noted. Also at steady state, the pressure profile is linear and the liquid saturation is uniform and constant between 30 and 35%, a value that is about 10 saturation units above connate. The steady-state liquid saturation is practically independent of flow rate and inlet foam quality. Hence, foam flow resistance is not a unique function of liquid saturation.

Steady-state flow behavior of foam is rationalized in terms of changes in bubble texture. We also suggest a unique way of plotting foam flow behavior such that all our data collapse to a single constant which is characteristic only of the porous medium and the stabilizing surfactant package. If proven general, this correlation should be very useful for estimating foam mobilities as input to numerical simulations of possible field applications.

References and illustrations at end of paper.

INTRODUCTION

Foam is a promising fluid for achieving mobility control in a variety of underground processes including enhanced oil recovery by steam, CO_2 , or enriched hydrocarbon flooding, and aquifer storage of natural gas or air. Because of its dispersed nature, foam exhibits low flow mobilities which may possibly overcome gravity override and viscous fingering through the permeable streaks always present in underground porous media.

Unfortunately, the flow behavior of foam is very complicated; there is a plethora of results that are directly contradictory. For example, Huh and Handy [1] report increasing foam mobility with increasing liquid velocity while Nahid [2] and Sanchez and Schechter [3] report the opposite. Also, Sanchez and Schechter [3] and Treinen, Brigham, and Castanier [4] observe hysteresis in foam mobility whereas Huh and Handy [1] do not. Both Huh and Handy [1] and Sanchez and Schechter [3] show that foam mobility (plotted as foam relative permeability) varies with the liquid saturation in the core. But De Vries and Wit [5] find a constant liquid saturation in the porous medium; they measure varying foam mobilities at this fixed saturation value.

Clearly, additional experiments are needed to resolve some of these discrepancies. Particularly needed are data in reservoir sandstones and at pressures close to reservoir conditions. Our goal is to understand foam flow behavior under these conditions in both the steady and unsteady states. Because of the contradictory results noted above, we desired a direct measure of the in-situ liquid saturations, and we wished to probe the possible separate effects of gas and liquid flow rates and hysteresis on foam flow behavior. Our experiments to meet these goals are described below.

EXPERIMENT

Apparatus

The experimental flow apparatus is shown in Fig. 1. A 5.1-cm (2-in.) diameter, 60-cm (24-in.) long core of Boise sandstone was epoxy-mounted into a 316 stainless steel cylinder designed for 20 MPa (3000 psia). The core porosity was 0.25 and one pore volume (PV) corresponded to 300 cm³. Swagelok O-seal pressure taps were drilled through the epoxy to the core, and liquid-filled tubes were connected from each pressure tap to a multiplexing valve. Pressure was measured using a single Paroscientific 43KT piezoelectric quartz-crystal pressure transducer (Paroscientific, Redmond, WA) and a Scanivalve 12L7 multiplexing valve (Scanivalve, San Diego, CA) set to visit sequentially all the taps. Back pressure was maintained by a Mity-mite dome-loaded back-pressure regulator (Grove Valve and Regulator Co., Emeryville, CA). Aqueous liquid was injected at a controlled rate by an LDC mini-pump, Model 2396 (Milton Roy Corp., Riviera Beach, FL). Nitrogen gas was injected at controlled mass flow rate through a Brooks 5850-TRP mass flow controller (Emerson Electric, Hatfield, PA).

Liquid saturation was measured by gamma-ray densitometry [6], using a 47 mCi Cs-137 source collimated to a 0.32-cm (1/8-in.) diameter beam, with detection by a Harshaw 5.1-cm (2-in.) NaI(Tl) scintillation counter and an NB-15X plug-on preamplifier (Harshaw Chemical Co. Solon, OH). Actual counting was done on a Norland IT-5300 multichannel analyzer (Norland Corp., Ft. Atkinson, WI), with a digital gain stabilizer to compensate for drift. The intensity of the gamma ray (counts/s falling within a 662 keV peak) was premeasured at selected stations when the core was at 0% and again at 100% liquid saturation. Liquid saturation was calculated from observed beam intensity using the relationship $S_{liq} = [\ln(I_d/T)]/[\ln(I_d/I_w)]$, where I_d and I_w are the intensity of the gamma ray premeasured at 0% and 100% liquid saturation, respectively, and I is the intensity measured at any unknown intermediate saturation. This relationship follows from the Beer-Lambert law [7]. The gamma-ray source and detector were mounted on a carriage which could be moved sequentially to each of the stations by a Slow-syn stepper motor and Model DPF107 motor controller (Anaheim Automation, Anaheim, CA). The greatest source of error in measurement of liquid saturation is the measurement of gamma-ray intensity. When counting radioactive decay, the standard deviation of the number of events counted is the square root of the number of events counted. Therefore the longer the counting period, the more precise is the measurement of liquid saturation. Because of the trade-off between counting time and precision in monitoring liquid saturation, it was necessary in transient measurements to choose between monitoring at one location with good time resolution or sweeping the length of the core with poorer resolution. Generally, we counted long enough to keep the standard deviation in liquid saturation to less than 5 saturation units during transient measurements and 2 saturation units during steady-state measurements. Pressure sweeps could be made without loss of time resolution. All measurements were controlled and data recorded by an HP-9000 series computer.

Steady-state relative permeabilities of the core to gas and liquid were measured in the drainage mode, with local effective permeabilities calculated between each pair of adjacent

pressure taps. The measured relative permeabilities are shown in Fig. 2. An arrow indicates the location of connate water saturation where it was not possible to gauge any liquid weepage.

The foamer solution was a brine containing 18.2 g/L Na, 1.3 g/L Mg, 5.4 g/L Ca, and 40.3 g/L Cl, with 1% by weight active surfactant. The surfactant was either of two chemically similar alkylethoxysulfates: Enordet AES 1215-9S (Shell Chemical Co.) or Steol 7N (Stepan Chemical Co., Northridge, IL). The surface tension, measured by the Wilhelmy plate method, was 29 mN/m; the viscosity, measured with a Contraves rotational viscometer, Model 15T, was 1.2 mPa·s. In some runs, 0.2 wt % of long chain alcohol of average carbon number 14 (Neodol 25) was added, which increased the liquid viscosity to 1.7 mPa·s.

Procedure

The core was initially vacuum-saturated with brine and displaced by at least 10 PV of foamer solution. In all runs, liquid was injected at constant volumetric rate and gas was injected at constant mass flow rate. The progress of gas and foam through the core was monitored by frequent pressure sweeps and by monitoring of liquid saturation at a single station, with occasional saturation sweeps. After foam had propagated through the length of the core and steady state was reached, the gas and liquid flow rates were varied independently to reach a series of steady states.

Gas flow velocity was calculated by converting the measured flow rate, in volume at standard conditions, to the average pressure in the core, and then dividing by the cross-sectional area of the core. The fractional flow of gas (also referred to as inlet foam quality) and the time per pore volume were also based on the average gas pressure in the core.

RESULTS

In this section we first report on the transient behavior when gas and liquid are injected and foam is propagated through the core. Then we examine the steady-state behavior as gas and/or liquid flow rates are changed stepwise. Here the goal is to determine the effects of changing flow rates upon foam mobility and liquid saturation.

Transient Behavior

Figures 3 through 5 show displacement results for simultaneous injection of aqueous surfactant solution and nitrogen at a fractional gas flow or inlet foam quality of 96% and a total superficial velocity of 4.2 m/day into the Boise sandstone core initially saturated with the surfactant solution. Transient liquid saturations in the sandstone are seen in Figs. 3 and 4 while Fig. 5 reports the corresponding pressure profiles.

From Fig. 3, which shows the liquid desaturation history at the 9.1-cm core location ($x/L = 0.15$), we observe monotonic decline to a steady value of 30% for times between 0.3 and 0.7 PV. For other positions we find an initial rather sharp decline to a saturation of about 65% followed by a gradual decline to the steady value. This is reminiscent of the two-step displacement process hinted at by Mohammadi, Van Slyke, and Ganong [8].

Figure 4 indicates that after the 65% liquid saturation front passes, desaturation occurs from the front of the core.

Gas breakthrough is observed near 1.0 PV. Sometime after 13 PV steady state is attained. The final liquid saturation in the core is about 30%, which from Fig. 2 is about 5 saturation units above connate saturation.

An important finding from Fig. 5 is that the transient pressure profiles exactly track the liquid-saturation history in that high pressure gradients (i.e., large foam flow resistances) occur where liquid saturations are lowest. For example, at the 1.03 PV time, which is close to gas breakthrough, the effective flow resistance is highest near the core inlet where the liquid saturation is 30%, while near the core outlet, where the liquid saturation is 65%, pressure gradients are quite small. The finding of low transient foam mobility at low liquid saturation is general for all core locations during the entire time of the displacement process. Mohammadi, Van Slyke, and Ganong [8] also indicated high foam mobility initially, followed by lower foam mobility during the latter stages of the displacement process. Again from Fig. 5, steady state is reached after 13 PV. The final pressure profile is linear, reflecting a constant foam mobility along the core.

In our transient studies, which are not extensive, we find that liquid displacement does not always behave in exactly the same fashion at each location in the core for different experiments. Likewise, the time to reach steady state varies. Usually several PV are sufficient, but in some experiments tens of PV are required. However, the following trends are invariably seen. There is a relatively rapid desaturation front at 65% liquid saturation, followed by a gradual displacement to near 35% commencing from the core inlet. Most of the time to reach steady state is during the second slow desaturation stage. During the transient displacement foam mobility is low where liquid saturation is low, and high where liquid saturation is high. Finally, a steady state is reached in which the pressure gradient and liquid saturations are practically uniform along the core. The final low foam mobilities and low liquid saturations indicate clearly that the minimum critical velocity necessary to generate a fine-textured, strong foam [9,10] was exceeded in all our experiments.

Steady Behavior

Figures 6 through 9 report the liquid saturation profiles and the relationship between pressure drop and flow rate in the steady state. The data cover a range of total superficial velocity between 1 and 45 m/day; the gas fractional flow at core average conditions ranges from 70 to over 99%. In these figures any numbers shown in parentheses refer to the gas fractional flow, or equivalently, to the inlet foam quality. Likewise, lines simply connect data points.

Figure 6 indicates that at a fixed liquid velocity and for a wide range in gas velocity, the liquid saturation in the core is constant. Except for the very lowest gas velocity, at which steady state has possibly not been reached, the liquid saturation is fixed at 30-35%. Clearly with foam flow there is not a 1 to 1 correspondence between fractional flow and liquid saturation.

Figure 7 shows the fascinating result that, for a fixed liquid velocity, the pressure drop is essentially independent of gas flow rate over a change of almost two orders of magnitude. De Vries and Wit find the same rheological behavior for foam flow in both sandstone and sandpacks at elevated pressure [5]. Conversely, Friedmann, Chen, and Gauglitz ascertain a $2/3$

power dependence of pressure drop on flow rate, although they consider much higher velocities than in this work [10].

Results for the effect of liquid velocity at constant gas velocity are shown in Figs. 8 and 9. Similar to Fig. 6, the steady-state saturation profiles in Fig. 8 are uniform and constant independent of liquid velocity down to a quality of 70%. This trend of constant liquid saturation for changing foam mobility needs to be studied for even wetter foams, but it again emphasizes that the mobility of foam is not a unique function of saturation.

Figure 9 displays the role of liquid velocity on foam pressure drop for two fixed gas velocities. Except at the lowest velocities, there is an almost linear increase in the foam pressure gradient with increasing liquid velocity. Again, Nahid [2] and Sanchez and Schechter [3] find a similar decrease in foam mobility with increasing liquid flow, but Huh and Handy [1] report just the opposite trend. Note that the two data points for the lower gas velocity fall on the same line as those for the higher gas velocity. This confirms the results of Fig. 7 that gas velocities do not have a major impact on the foam pressure drop.

The letters in alphabetic order labeling the points in Fig. 9 indicate consecutive steady states. Either raising or lowering gas or liquid flow to the same final state produces identical flow behavior. We do not observe hysteresis in steady-state foam mobilities.

DISCUSSION

Foam in porous media is a gas (or internal nonwetting phase) dispersed in an interconnected wetting liquid comprised of liquid bridges and lamellae [9,11]. During flow, the injected gas and liquid phases, whether initially dispersed or not, separate near the core inlet. Wetting liquid occupies the smallest pores and transports separately from the foam phase. The amount of wetting liquid conducted by flowing lamellae and liquid bridges and through and along static lamellae is very small compared to that conducted by the completely liquid-filled pore channels [12,13]. Consequently, the quality of the foam phase inside a porous medium is higher than that injected. Further, the wetting liquid-flow resistance obeys the classic two-phase Darcy's law. At a given wetting-liquid saturation, the relative permeability to the liquid is the same as that in two-phase flow of immiscible Newtonian fluids, independent of the presence of a discontinuous foam phase. Essentially all investigations of foam flow in porous media confirm this observation [1,3,5,13-15].

Because the wetting liquid separates into its own pore channels, the foam phase becomes the nonwetting phase and transports in the large pores not occupied by the continuous wetting liquid. The foam phase can be classified according to three regimes: trapped bubble trains, flowing bubble trains, and possibly, for weakly stabilizing surfactants or high gas velocities, free continuous gas. The three regimes are listed qualitatively in increasing order of the pore sizes in which they reside. From visual observations of etched-glass micromodels, non-flowing foam is trapped at pore constrictions [16] and therefore occupies the intermediate size pores. Tracer [2,10,13] and micromodel [16] experiments provide estimates of the fraction of the foam phase that is trapped between 30 and 90%. Flowing bubbles are located in the next largest pore channels, with

any free gas likely occupying the very largest pores.

The most important property that determines the amount of trapped (versus flowing) foam and the effective flow resistance of each regime is the texture (i.e., the bubble size and size distribution) [11]. Micromodel studies [9,16-18] and core effluent observations [15,19] of texture indicate that the bubble size distribution exhibits a wide spread. Bubbles can be significantly smaller or larger than pore bodies but generally they are on the order of one to several pore body volumes (see, for example, Fig. 1 of [20]). The discontinuous gas bubbles essentially span the pores channels in which they reside, and, when flowing, they slide over thin films and crevices of wetting liquid adjacent to mineral grain surfaces [16,20,21]. Considerable success has been achieved in predicting flowing bubble resistance based on elongated bubbles flowing in a single capillary and a linear dependence on local bubble density [10,19,21,22]. Similarly, initial attempts at understanding bubble trapping and the pressure gradients necessary to release bubbles also involve the bubble texture [23]. Foam microstructure in the porous medium directly determines its flow resistance.

Bubbles do not maintain their identity during transport through a porous medium. Whether externally generated or produced inside the core, they are shaped according to the nature of the porous medium in which they find themselves by "making" and "breaking" processes [4]. Foam texture arises from a balance among varied and complicated mechanisms which give rise to bubble birth and death. Lamellae and bubbles are generated primarily by snap-off in intermittently liquid-filled germination sites [9,16,17,24] (two other generation mechanisms are leave-behind and bubble division [9]). Conversely, lamellae break from capillary suction at Plateau borders [20,25], from fast and extensive stretching near pore bodies of termination sites [20] and from gas diffusion between adjacent bubbles of different mean curvatures [15,26].

For an effectively incompressible foam generated inside a linear core, the bubble texture diminishes over quite small distances to a constant steady-state size where the rates of generation and collapse are equal [10]. At this state even the trapped bubble trains should not be viewed as completely static. Ever-present pressure fluctuations and flow-path alterations release some trapped bubble trains. These are subsequently replaced from the flowing bubble regime at equal frequency.

The kinetics of foam generation and collapse obviously depend upon surfactant structure, composition, and concentration, but they also depend upon liquid saturation [9,20], and separately on gas and liquid flow rates [10,15,19,20]. Because of the velocity rate effects and the redistribution of the wetting liquid into its own flow paths, foam mobility is not in general expected to be a unique function of fractional flow or saturation. Additionally, because the foam making and breaking kinetics vary with velocity, the foam texture does also. This re-emphasizes how strongly foam texture and foam rheology are coupled.

Based on these general observations we now discuss our transient and steady-state experimental results.

Transient Behavior

To rationalize the transient displacement results of Figs.

3-5, we tentatively argue as follows. Initially, unfoamed gas fingers into the larger pore channels because of extremely adverse mobility contrast. Foam bubbles and lamellae are created by leave-behind and by snap-off. However, their number density is small because germination sites are sparse in the large pore space [9] and because the locally high interstitial gas velocities may destroy some moving lamellae [20]. This rather coarse-textured, weak foam does exhibit some increased flow resistance compared to the free gas [9]; accordingly, the local pressure gradients increase (for constant imposed flow rates) enough to overcome the entrance capillary pressure of nearby liquid-filled pores. More liquid is now displaced, allowing the gas to encounter additional germination and leave-behind sites. Bubble and lamellae density further increase, which again raises local pressure gradients, and so on in a cascading fashion.

Wetting-fluid displacement is faster early at high liquid saturation compared to that later at low liquid saturation because the capillary entrance pressures at high liquid saturations (i.e., those reflecting larger pore throats) change much more gradually per unit of desaturation compared to those at low liquid saturations. Relatively larger flow pressure gradients are therefore demanded for desaturation at low liquid saturation. These higher pressure gradients require a finer-textured foam, which takes longer to evolve. This reasoning also explains why the high pressure gradients in Fig. 5 correspond directly to the low liquid saturations in Fig. 4. Finally, at steady state a strong foam [9] of constant and fine texture (i.e., high flow resistance) develops throughout the core, forcing the liquid saturation down to a low and uniform value and establishing a uniform pressure gradient (i.e., a linear pressure profile).

Of course, even at steady state there must be a net bubble generation near the core inlet and a decline in bubble size. Apparently, the region where the rates of bubble birth and death are out of balance is confined to a region so near the core inlet that it does not affect the overall linearity of the pressure profile. De Vries and Wit state a similar conclusion [5], although Minssieux detected a region of high liquid saturation near the inlet of a sandpack [27].

The lack of precise reproducibility for transient displacement by foam may be due to the chaotic nature of the initial gas-fingering process. Somewhat different gas flow paths are likely established for each separate experiment. Foam evolution is therefore somewhat statistical. Fortunately, steady-state behavior does appear to be reproducible.

The foam-flooding process is unique in that the drive fluid becomes more flow resistant or thickens with time. In the unsteady state, foam may thus be classified as rheopectic. Near the flood front free gas exists, behind the front coarse or weak foam exists, and still further behind the front a strong, fine-textured foam evolves. According to this scenario, use of the Johnson-Bossler-Naumann technique [28] to calculate unsteady relative permeabilities of foam from dynamic displacement data seems ill-advised. Not only is the rheopectic nature of foam ignored, but the Johnson-Bossler-Naumann procedure implicitly presumes that both the drive and displaced fluids exhibit flow resistances that are unique functions of local saturation. This presumption is not correct even for foam

flowing at steady state, as discussed below.

Steady Behavior

Over the range of flow velocities and fractional flows that we have investigated, once a strong foam evolves at steady state, the liquid saturation is driven down to about 35%. This value is independent of fractional flow and velocity. Foam mobility varies at this constant saturation. Figures 10 and 11 show the separate dependences of foam resistance on gas and liquid velocities, respectively. We choose to report our results in terms of a nondimensional foam flow resistance, FFR, defined by

$$FFR \equiv \frac{k}{\mu_{liq} v_{gas}} \left(\frac{-dp_{gas}}{dx} \right) \quad (1)$$

where k is the absolute permeability, p_{gas} is the gas pressure, v_{gas} is the gas superficial velocity, x is the axial distance along the core, and μ_{liq} is the wetting-liquid viscosity. FFR may be considered either as a foam flow resistance or as an inverse foam mobility, both made nondimensional by the absolute permeability and the liquid-phase viscosity. Figures 10 and 11 replot the data of Figs. 7 and 9, respectively, in terms of FFR.

Figure 10 indicates that at constant liquid velocity foam is a shear-thinning fluid: higher gas velocities reduce FFR. The simplest models of the flowing bubble-train regime reveal that at constant texture the pressure drop should vary with gas velocity to the $2/3$ power [11,21,22], as observed by Friedmann, Chen, and Gauglitz [10]. This means that FFR should vary with gas velocity to the $-1/3$ power. Because of the insensitivity of gas pressure gradient to gas velocity, however, Fig. 10 reveals a -1 power dependence, or a much more strongly shear-thinning foam.

At least three explanations may be offered. First, higher gas velocities could coarsen the foam texture. The reason is that processing more gas through a fixed number of germination sites (recall that the liquid saturation is constant) of constant snap-off frequency produces larger bubbles and decreases bubble density. Further, higher gas velocities lead to faster coalescence, also coarsening the foam [20]. Second, additional fluid-mechanical resistances, such as viscous dissipation in stretching and contracting lamellae, could contribute to the foam rheology. Third, the higher pressure gradients at higher gas velocities could release trapped bubbles and open more flow channels. However, this latter effect of trapped-bubble release should not be significant because of the relatively constant pressure gradient independent of gas velocity (cf. Fig. 7).

From Fig. 11 we discover that foam flow at constant gas velocity appears to be approximately Newtonian. That is, FFR increases almost proportionally with increasing liquid velocity. The proposed explanation is that the higher liquid velocities through germination sites increase the frequency of snap-off, making more bubbles and a finer textured foam. Thus, liquid velocity influences the foam mobility indirectly through bubble density.

The observations in Figs. 7 and 9 that foam pressure gradients increase about linearly with liquid velocity and are reasonably independent of gas velocity suggest that FFR is directly proportional to v_{liq}/v_{gas} . This means also that FFR^{-1}

(i.e., the effective foam flow mobility) is directly proportional to f_{gas}/f_{liq} , independent of total velocity. Thus a plot of FFR^{-1} versus total velocity should yield horizontal lines for constant values of fractional gas flow, with the spacing between the lines increasing as fractional gas flow increases. Lee and Heller [29] report plots for CO_2 foam that seem to show this behavior, except possibly at the highest gas fractional flows (see Figs. 3 and 4 of [29]).

Because we find that FFR is proportional to v_{liq}/v_{gas} , the quantity $FFR(v_{gas}/v_{liq})$ should be a constant independent of fractional flow and total velocity, as shown in Fig. 12. There does appear to be a slight upward trend toward high foam qualities, consonant both with the deviations from linearity in Fig. 9 at low liquid velocity and with the deviations seen by Lee and Heller [29]. Nevertheless, if proven general, the correlation suggested in Fig. 12 should be extremely useful for practical estimates of foam flow behavior. With only one or two measurements of foam pressure drops and flow rates in a given porous medium and with a given surfactant system (i.e., to set the absolute level of $FFR(v_{gas}/v_{liq})$), the entire steady flow behavior of foam can be predicted. We caution that a wider range of foam qualities, and different core permeabilities and surfactant types and concentrations must be studied before such a correlation can be solidified.

Finally, Fig. 13 repeats the general finding in foam-flow studies that the liquid flow resistance obeys Darcy's law. Here the liquid relative permeability is plotted as a function of gas fractional flow for several different liquid and gas flow rates. A constant value of about 10^{-3} emerges. This value is very close to that measured independently in two-phase flow of continuous gas and surfactant-free brine in Fig. 2 at the wetting-liquid saturation of 30-35%. Hence increasing (or decreasing) liquid flow rates during steady flow of strong foam simply forces more (or less) liquid through the liquid-filled channels. The number of liquid paths is not materially changed.

The attentive reader will note that $FFR(v_{gas}/v_{liq})$ and the inverse relative permeability to the liquid phase are identical (i.e., compare the constant values in Figs. 12 and 13). This follows immediately because at steady state the identical pressure gradients in the wetting and nonwetting phases for the velocity-weighted resistances to be identical. The underlying reason why both $FFR(v_{gas}/v_{liq})$ and the inverse relative permeability to the liquid phase are constant is that the liquid saturation remains constant independent of both the gas and liquid velocity.

In summary, foam flowing in porous media is a rheopectic fluid which at steady state is pseudoplastic with respect to gas flow and Newtonian with respect to liquid flow. Foam exhibits fascinating multiple personalities. Apparently, the foam texture adjusts to set a flow resistance that is compatible with a constant and low liquid saturation in the core. Because of the strong coupling between foam flow and foam texture, progress at quantifying the rheology of this unique fluid [10] can only be made by directly measuring bubble-size distributions.

CONCLUSIONS

We make the following conclusions for foam flow in

1 μm^2 sandstone at about 5 MPa (700 psia) back pressure and for total superficial velocities between 1 and 45 m/day and foam quality between 0.7 and 0.995:

1. During transient foam flooding of a surfactant-solution-saturated core, the foam flow resistance builds in time and continuously varies from that characteristic of free gas to that of a strong, fine-textured foam.
2. Steady foam flow resistance increases with increasing liquid velocity but decreases with increasing gas velocity. No hysteresis is observed in the steady state.
3. Although foam flow resistance varies with flow rate, liquid saturations at steady state do not. They are constant at 0.3 to 0.35 independent of flow rates and foam quality. Therefore, foam flow resistance is not a unique function of liquid saturation.
4. Liquid flow resistance during foam flow obeys Darcy's law and exhibits the standard relative permeability pertinent to the core liquid saturation, independent of liquid and gas flow rates.
5. A unique flow-resistance correlation is suggested which collapses all our data into a single value. This value is characterized only by the nature of the porous medium and the stabilizing surfactant package and is independent of foam quality and total velocity.
6. The most crucial parameter controlling foam flow resistance in porous media apparently is the bubble texture.

NOMENCLATURE

- f = fractional flow (dimensionless)
 FFR = $\frac{k}{\mu_{\text{liq}} v_{\text{gas}}} \left(\frac{-dp_{\text{gas}}}{dx} \right)$ nondimensional foam flow resistance
 I = intensity of gamma-ray radiation (counts/s)
 k = absolute permeability (μm^2)
 L = core length (m)
 p = pressure (Pa)
 S = saturation (dimensionless)
 v = superficial velocity (m/s)
 x = distance along core (m)

Greek letters:

μ = viscosity (Pa·s)

Subscripts:

- d = 0% liquid saturation
 w = 100% liquid saturation

ACKNOWLEDGMENTS

This work was supported by the Gas Research Institute, Chicago, IL, under Contract No. 5086-271-1160, and by the U.S. Department of Energy, under Contract No. DE-AC03-76SF00098 to the Lawrence Berkeley Laboratory of the University of California.

REFERENCES

1. Huh, D. G. and Handy, L. L.: "Comparison of Steady and Unsteady-State Flow of Gas and Foaming Solution in Porous Media," SPE 15078, presented at the 1986 California Regional Meeting of the SPE, Oakland, CA, April 2-4.
2. Nahid, B. H.: "Non-Darcy Flow of Gas through Porous Media in the Presence of Surface Active Agents," Ph.D. Thesis, University of Southern California, Los Angeles, CA., (1971).
3. Sanchez, J. M. and Schechter, R. S.: "The Effect of Trace Quantities of Surfactant on Nitrogen/Water Relative Permeabilities," SPE 15446, presented at the 1986 Annual Technical Conference and Exhibition of the SPE, New Orleans, LA, October 5-8.
4. Treinen, R.J., Brigham, W.E., and Castanier, L.M.: "Apparent Viscosity Measurements of Surfactant Foam in Porous Media - SUPRI TR-48," U.S. Dept. of Energy Report DOE/SF/11564-13 (DE86000260), December 1985.
5. DeVries, A. S. and Wit, K.: "Rheology of Gas/Water Foam in the Quality Range Relevant to Steam Foam," SPE 18075, presented at the 1988 Annual Technical Conference and Exhibition of the SPE, Houston, TX, October 2-5.
6. Reda, D.C. and Eaton, R.R.: "Definition of a Facility for Experimental Studies of Two-Phase Flows and Heat Transfer in Porous Material," AIAA 16th Thermophysics Conference, Paper No. AIAA-81-1190 (1981).
7. Moore, W.J.: *Physical Chemistry* 3rd ed, Prentice-Hall, Englewood Cliffs, NJ (1963) p. 820.
8. Mohammadi, S.S., Van Slyke, D.C., and Ganong, B.: "Steam-Foam Pilot Project in Dome-Tumbador, Midway Sunset Field," paper SPE 16736 presented at the 1987 Annual Technical Conference and Exhibition of the SPE, Dallas, TX, September 27-30.
9. Ransohoff, T. C. and Radke, C. J.: "Mechanism of Foam Generation in Glass-Bead Packs," *SPE* (May 1988) 573-585.
10. Friedmann, F., Chen, W. H. and Gauglitz, P. A., "Experimental and Simulation Study of High-Temperature Foam Displacement in Porous Media," SPE/DOE 17357, presented at the 1988 SPE/DOE Enhanced Oil Recovery Symposium, Tulsa, OK, April 17-20.
11. Falls, A.H., Hirasaki, G.J., Patzek, T.W., Gauglitz, P.A., Miller, D.D., and Ratulowski, T.: "Development of a Mechanistic Foam Simulator: The Population Balance and Generation by Snap-Off," *SPE* (August 1988) 884-892.

12. Bond, D.C. and Bernard, G.G.: "Rheology of Foams in Porous Media," presented at the 1966 SPE-AIChE Joint Symposium and AIChE 58th Annual Meeting, Dallas, TX, February 7-10.
13. Holm, L. W.: "The Mechanism of Gas and Liquid Flow Through Porous Media in the Presence of Foam," *SPEJ* (December 1968) 359-369.
14. Bernard, G.G., Holm, L. W., and Jacobs, W. L.: "Effect of Foam on Trapped Gas Saturation and on Permeability of Porous Media to Water," *SPEJ* (December 1965) 295-300.
15. Friedmann, F. and Jensen, J. A.: "Some Parameters Influencing the Formation and Propagation of Foams in Porous Media," SPE 15087, presented at the 1986 California Regional Meeting of SPE, Oakland, CA, April 2-4.
16. Manlowe, D. J.: "Pore-Level Mechanisms of Foam Destabilization by Oil in Porous Media," M. S. Thesis. University of California, Berkeley (1988), Appendix 4B, p. 186-189.
17. Mast, R. F.: "Microscopic Behavior of Foam in Porous Media," SPE 3997, presented at the 1972 Annual Meeting of SPE, San Antonio, TX, October 8-11.
18. Owete, O. S. and Brigham, W. E.: "Flow Behavior of Foam: A Porous Micromodel Study," *SPE* (August 1987) 315-323.
19. Ettinger, R.A.: "Flow Resistance of Foam in Berea Sandstone," M.S. Thesis, University of California, Berkeley, 1989.
20. Jimenez, A. I. and Radke, C. J.: "Dynamic Stability of foam Lamellae Flowing Through a Periodically Constricted Pore," presented at the Symposium on Advances in Oil Field Chemistry, Third Chemical Congress of the North American Continent and 195th National Meeting of ACS, Toronto, Canada, June 5-11 (1988).
21. Ginley, G. M. and Radke, C.J.: "The Influence of Soluble Surfactants on the Flow of Long Bubbles Through a Cylindrical Capillary," presented at the Symposium on Advances in Oil Field Chemistry, Third Chemical Congress of the North American Continent and 195th National Meeting of ACS, Toronto, Canada, June 5-11 (1988).
22. Hirasaki, G. J. and Lawson, J. B.: "Mechanisms of Foam Flow in Porous Media: Apparent Viscosity in Smooth Capillaries," *SPEJ* (April 1985) 176-190.
23. Rossen, W. R.: "Theories of Foam Mobilization Pressure Gradient," SPE/DOE 17358, presented at the 1988 SPE/DOE Enhanced Oil Recovery Symposium, Tulsa, OK, April 17-20.
24. Ransohoff, T.C., Gauglitz, P.A., and Radke, C.J.: "Snap-off of Gas Bubbles in Smoothly Constricted Noncircular Capillaries," *AIChE Journal* (May 1987) 753-765.
25. Khatib, Z.I., Hirasaki, G.J., and Falls, A.H.: "Effects of Capillary Pressure on Coalescence and Phase Mobilities in Foams Flowing Through Porous Media," *SPE* (August 1988) 919-926.
26. Bikerman, J.J.: *Foams*, Springer-Verlag, New York, NY (1973) p. 194.
27. Minssieux, L.: "Oil Displacement by Foams in Relation to their Physical Properties in Porous Media," *JPT* (January 1974) 100-108.
28. Johnson, E.F., Bossler, D.P., and Naumann, V.O.: "Calculation of Relative Permeability from Displacement Experiments," *Trans. AIME* 216 370-372 (1959).
29. Lee, H.O. and Heller, J.P.: "Laboratory Measurements of CO₂-Foam Mobility," paper SPE 17363, presented at the 1988 SPE/DOE Enhanced Oil Recovery Symposium, Tulsa, OK, April 17-20.

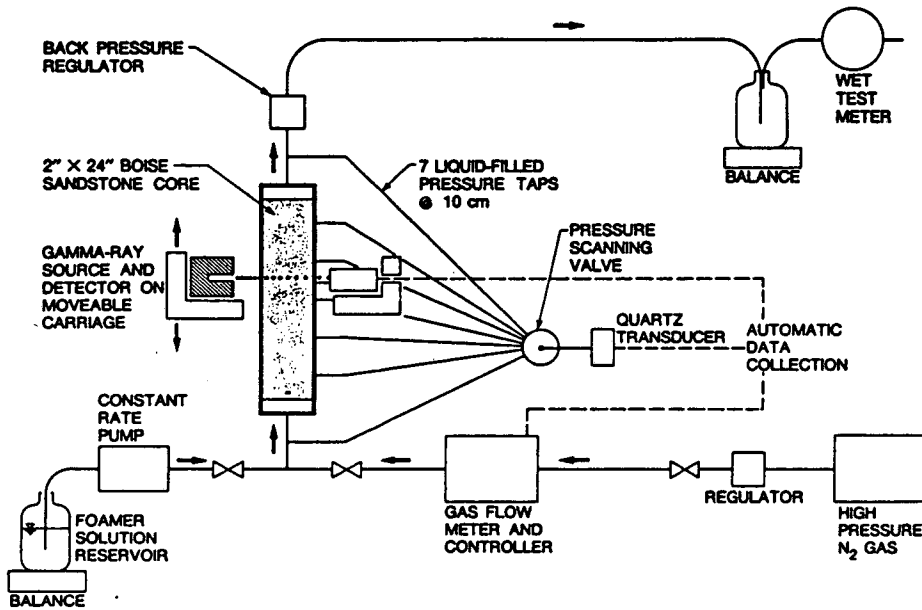


Fig. 1—Apparatus for foam flow experiments.

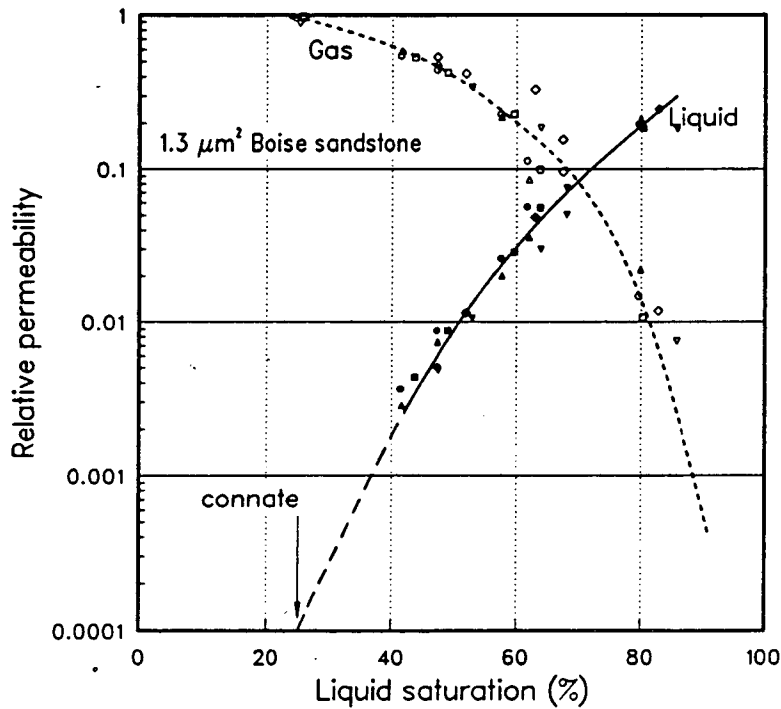


Fig. 2—Gas/brine relative permeability of Boise sandstone. Open symbols refer to gas and closed symbols to the liquid phase. Various symbols reflect individual measurements between each pair of adjacent pressure taps.

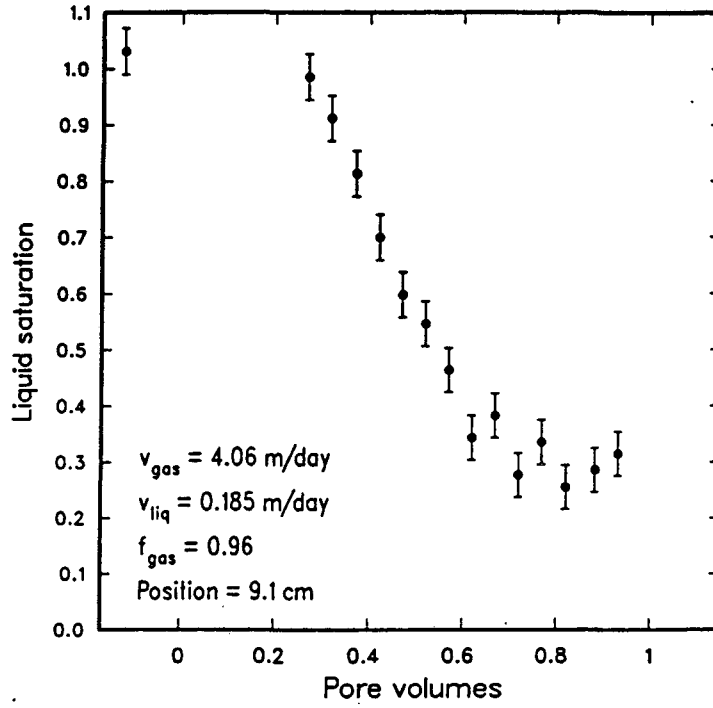


Fig. 3—Transient decrease in local liquid saturation during first pore volume of foam flooding. Liquid viscosity = 1.7 mPa·s.

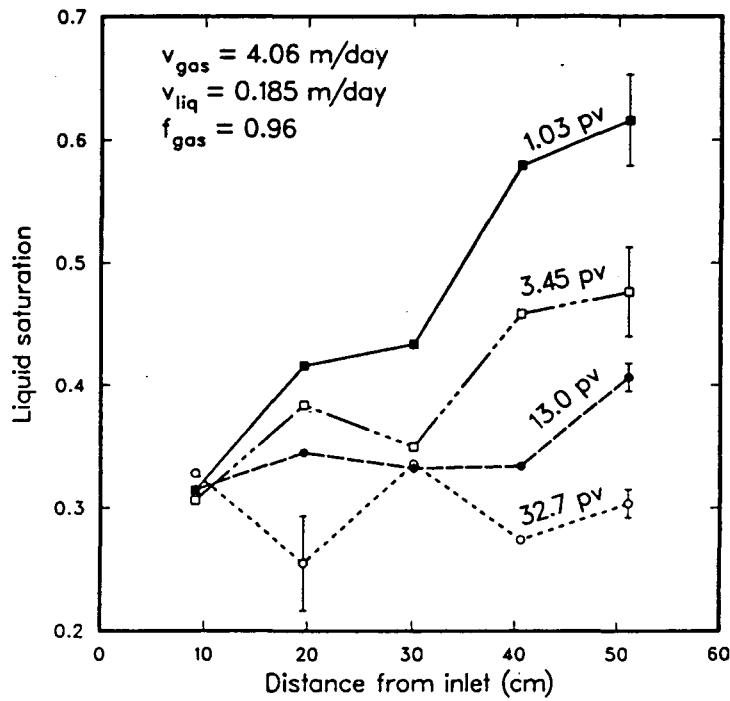


Fig. 4—Liquid saturation profiles measured during transient displacement of liquid by foam. Error bars shown at 51 cm are typical. Liquid viscosity = 1.7 mPa·s.

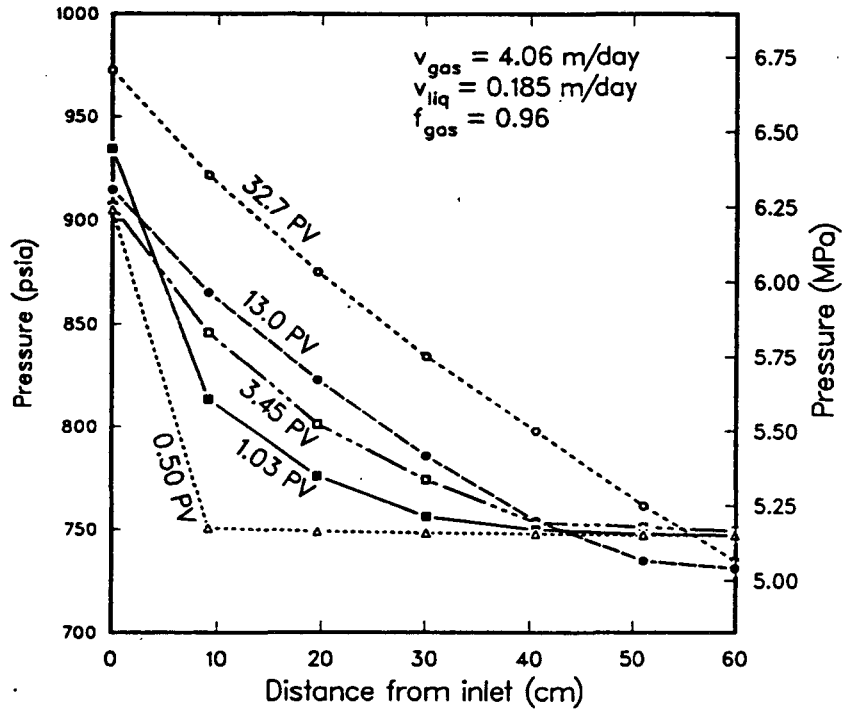


Fig. 5—Pressure profiles measured during transient displacement of liquid by foam. Liquid viscosity = 1.7 mPa·s.

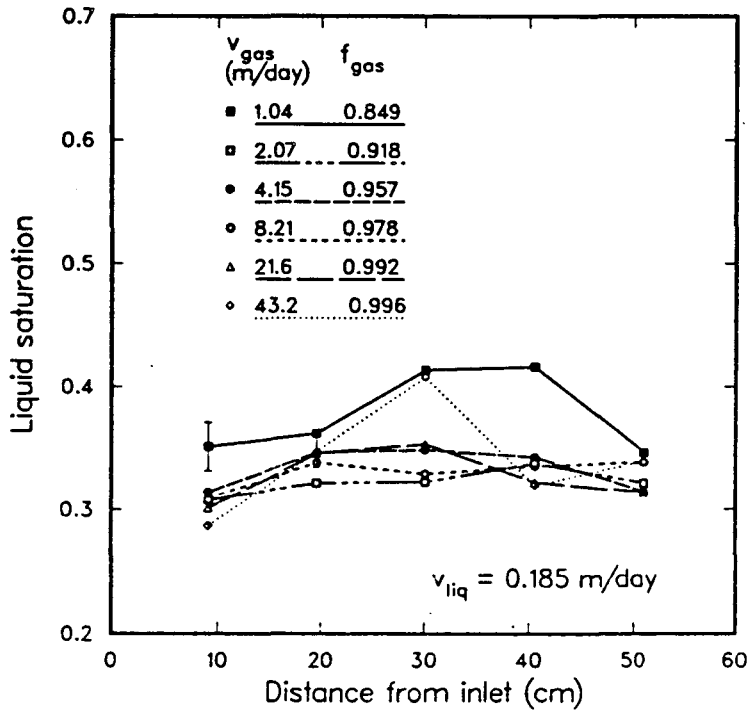


Fig. 6—Liquid saturation profiles measured during six successive steady states at different gas velocities. Liquid velocity held constant at 0.185 m/day; liquid viscosity = 1.7 mPa·s. The longer error bar is typical for measurements made with $v_{gas} = 1.04 \text{ m/day}$; the shorter error bar is typical for measurements made at all other gas velocities.

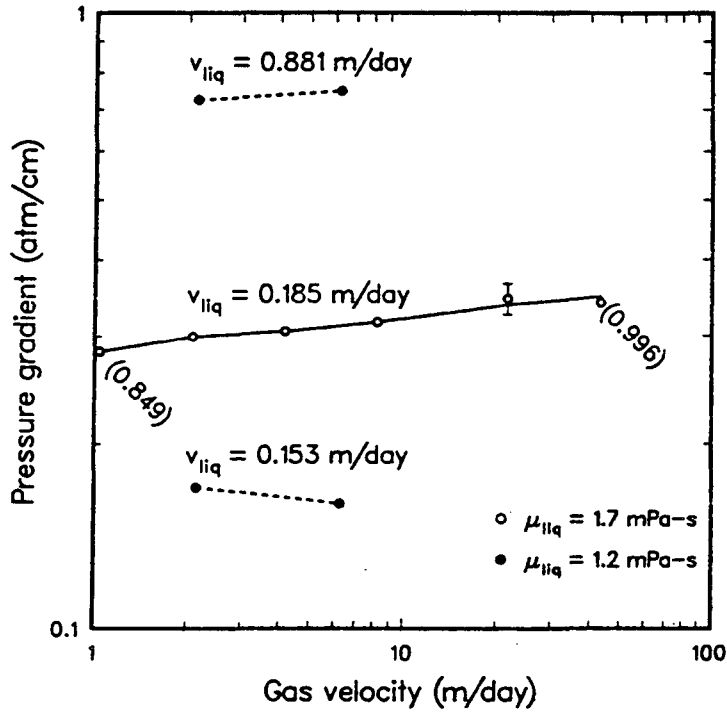


Fig. 7—Steady foam pressure gradient vs. gas velocity for three constant liquid velocities. Numbers in parentheses correspond to fractional gas flow. A typical error bar is shown.

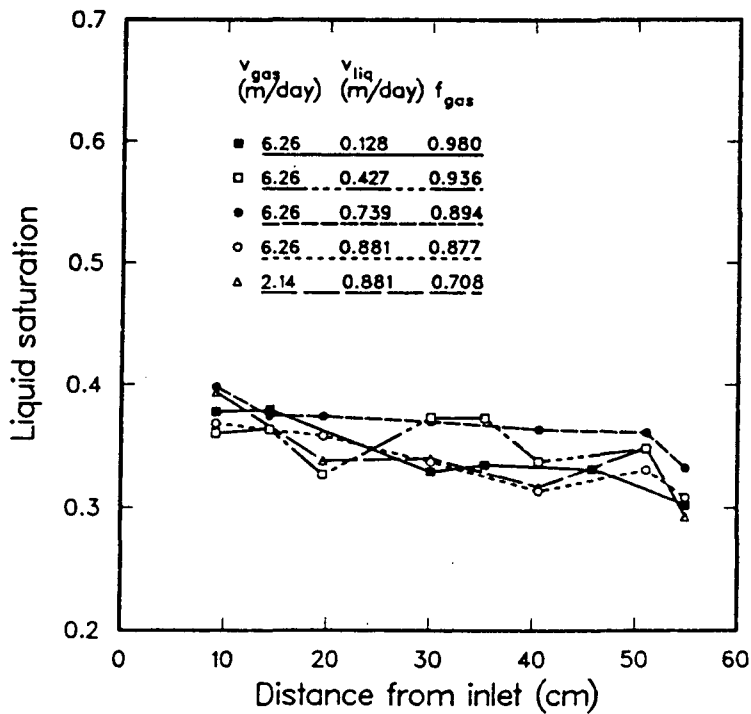


Fig. 8—Liquid saturation profiles measured during five successive steady states. These profiles correspond to points labeled A through E in Fig. 9. Uncertainty for all measurements is $\pm 2\%$. Liquid viscosity = 1.2 mPa · s.

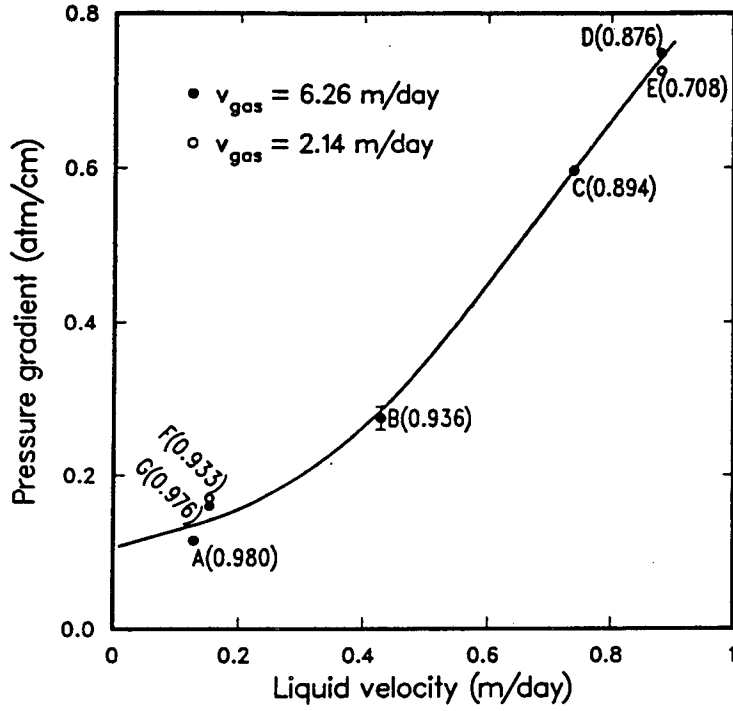


Fig. 9—Steady foam pressure gradient vs. liquid flow rate. Points labeled A through G represent consecutive steady states. Numbers in parentheses correspond to fractional gas flow. Liquid viscosity = 1.2 mPa·s. A typical error bar is shown.

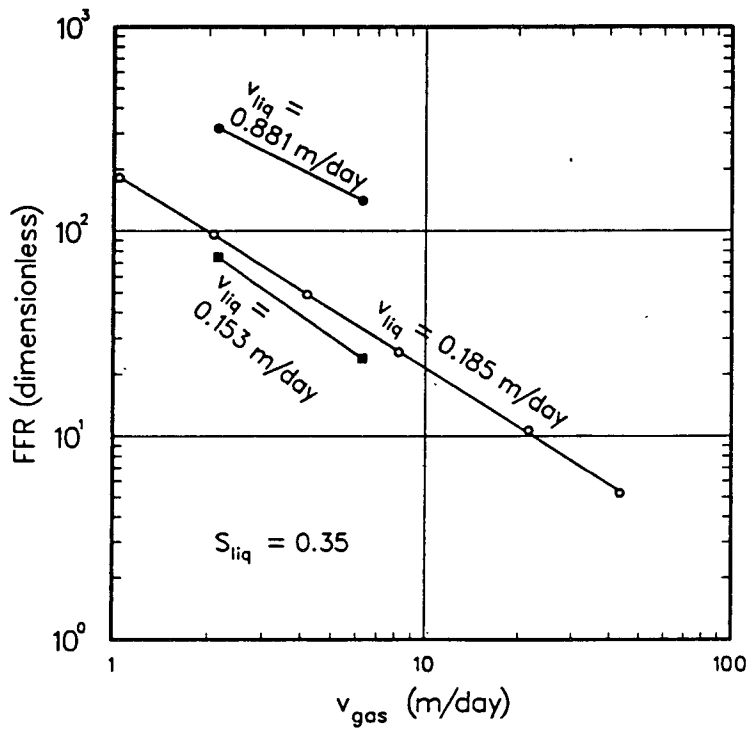


Fig. 10—Foam flow resistance vs. gas velocity.

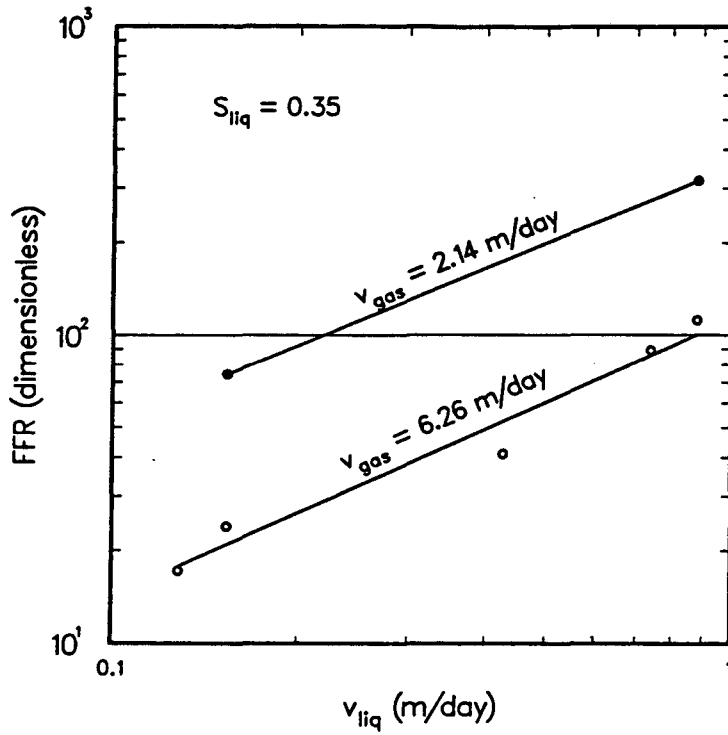


Fig. 11—Foam flow resistance vs. liquid velocity.

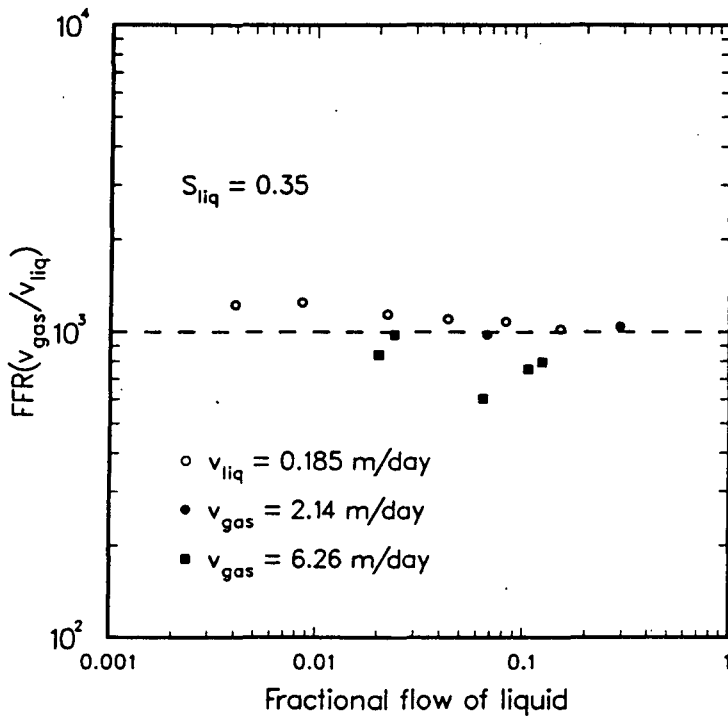


Fig. 12— $FFR(v_{gas}/v_{liq})$ vs. fractional flow of liquid. The dashed line is eye fit.

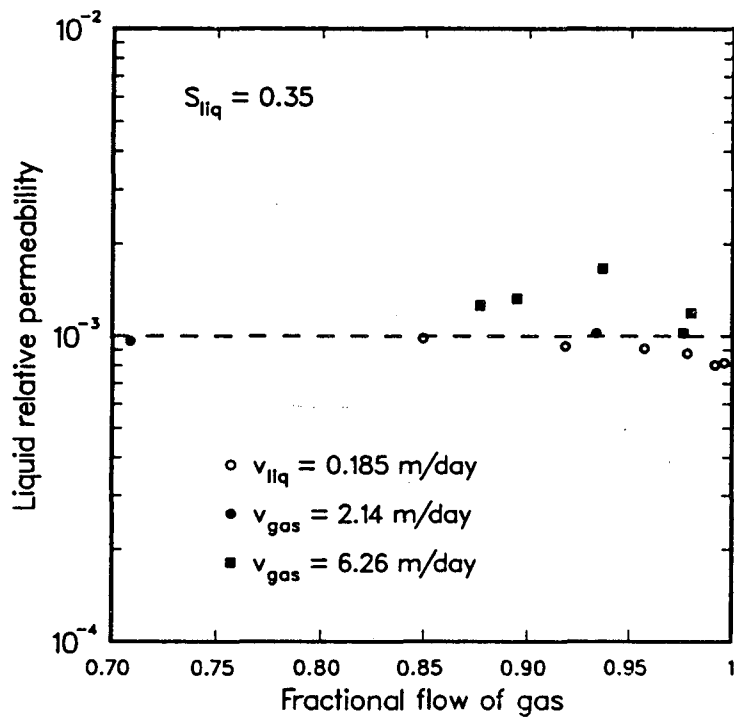


Fig. 13—Liquid relative permeability vs. fractional flow of gas. The dashed line is eye fit.

LAWRENCE BERKELEY LABORATORY
UNIVERSITY OF CALIFORNIA
INFORMATION RESOURCES DEPARTMENT
BERKELEY, CALIFORNIA 94720